STATIC AND DYNAMIC CHARACTERIZATION OF POROUS CARBON AEROSTATIC GAS BEARINGS

An Undergraduate Research Scholars Thesis

by

JOSE TORRES

Submitted to the Undergraduate Research Scholars program at
Texas A&M University
in partial fulfillment of the requirements for the designation as an

UNDERGRADUATE RESEARCH SCHOLAR

Approved by Research Advisor: Dr. Adolfo Delgado

May 2018

Major: Mechanical Engineering

TABLE OF CONTENTS

ABSTRACT

Static and Dynamic Characterization of Porous Carbon Aerostatic Gas Bearings

Jose Torres
Department of Mechanical Engineering
Texas A&M University

Research Advisor: Dr. Adolfo Delgado
Department of Mechanical Engineering
Texas A&M University

Gas bearings provide a variety of benefits including eliminating the need for oil, reducing power losses, enabling high speed operation, and reducing equipment footprint [1]. Gas bearings have been successfully used in small size turbomachinery, but implementation in larger machinery has proven difficult due to their limitations in dynamic performance and load capacity [2]. For example, hydrostatic gas bearings are susceptible to air-hammer instability, a phenomenon in which the compressibility of the gas creates a self-excited instability that can lead to bearing failure [3]. The purpose of this research project is to advance the state-of-the-art of process gas lubricated bearings for land-based turbomachinery applications. The main goal will be to experimentally characterize the static and dynamic performance of aerostatic gas films using porous carbon material as the gas delivery system. The proposed experiments are designed to identify stiffness and damping of porous carbon pads. The pads will be tested in a dynamic flat plate tester. Stiffness and damping coefficients can be calculated as a function of excitation frequency, applied load, and pressure ratio for multiple film thicknesses and inlet pressures. This paper will present simulated results for gas bearing static performance and discuss test

procedures that will be carried out to experimentally characterize static and dynamic gas bearing performance in the future.

ACKNOWLEDGEMENTS

The completion of this undergraduate thesis could not have been possible without the contributions of Dr. Adolfo Delgado and Harley May. Their guidance and assistance during this project is greatly appreciated.

NOMENCLATURE

m	Mass of Shaker Plate
C	Damping Coefficient of Gas Film
K	Total Stiffness Coefficient
y	Displacement of Shaker Plate
$\dot{y}$	Velocity of Shaker Plate
$\ddot{y}$	Acceleration of Shaker Plate
K_f	Gas Film Contribution to Stiffness Coefficient
K_{tb}	Turnbuckle Assembly Contribution to Stiffness Coefficient
$f(t)$	Load Applied to Gas Film
y_1	Height of Shaker Plate where Resistance from Gas Film Begins
y_0	Height of Shaker Plate at Contact with Bearing

CHAPTER I

INTRODUCTION

Gas lubricated bearings have generally been used in small high precision devices such as medical equipment, hard drives and hand tools [4]. Gas bearings offer several advantages when compared to oil bearings and rolling element bearings, including the ability to operate at high speeds while minimizing power losses and removing the need for active oil lubrication. Self-acting hydrodynamic bearings are the most common type of gas bearing used in turbomachinery applications. Hydrodynamic bearings utilize the rotational speed of the journal along with the viscosity of the lubricant (liquid or gas) to create a thin film between the journal and the bearing. One of the issues associated with self-acting gas bearings is the surface wear that occurs at machine start up before the journal reaches lift-off speed. An effective approach to eliminate wear at low speeds is to create a hydrostatic gas film using pressurized gas from an external source. The most common methods to supply pressurized gas to the bearing include external flow restrictors such as orifices or capillary restrictors, and in some cases a supply port discharging to a shallow recess to help increase load capacity [5]. One method that has not received in-depth attention and testing involves using porous material as the medium to supply pressurized gas to the system. Due to the porosity of the material, the pressure created in the thin film region can be distributed throughout the entire surface of the bearing. Porous carbon bearings have been extensively used for linear motion applications and, more recently, in small rotating devices and larger machines operating at sub-critical speeds (i.e. MRI gantry). The static performance of the bearing is well documented by vendors in terms of inlet pressure and pad porosity. However, to the extent of the research team's knowledge, there is currently no

published data identifying the static and dynamic performance of a gas film created through a porous carbon material. This information is required to evaluate the feasibility of using porous carbon (graphite) in oil-free turbomachinery bearings and will be the focus of this research project.

CHAPTER II

METHODS

Project Overview

The goal of this project is to characterize the static and dynamic performance of aerostatic gas films in porous carbon bearings. For small motions, the hydrostatic gas film is represented as a combination of a linear spring and damper elements, as shown in Figure 1. In this case, a porous carbon thrust bearing manufactured by New Way Air Bearings is used as the gas delivery source.

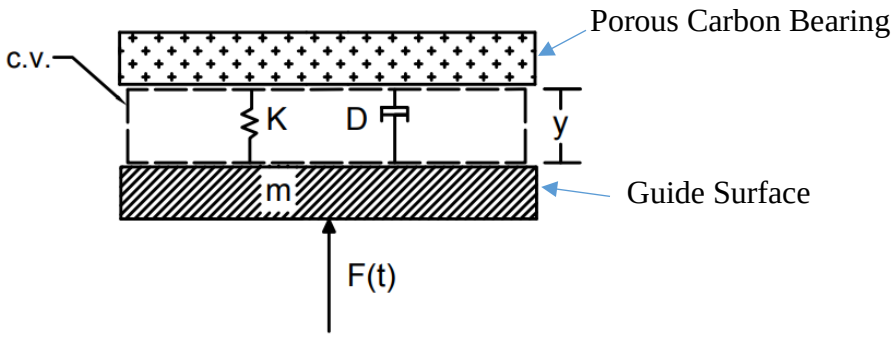

FIGURE 1: Spring-Mass-Damper System

Following this physical representation, the equation of motion of the spring-mass-damper system is governed by the following second order differential equation:

$$\boldsymbol{m\ddot{y} + C\dot{y} + Ky = f(t)} \qquad \textbf{(1)}$$

$$\boldsymbol{K = K_f + 4K_{tb}} \qquad \textbf{(2)}$$

Where *m* represents the mass of the system, *C* is the damping coefficient, *K* is the stiffness coefficient, *y* represents the displacement, and *f(t)* gives the applied force. The stiffness

will include contributions from the gas film and the turnbuckle assemblies as shown by Equation 2, which will be further discussed in the next section.

Static and dynamic testing in a flat plate test rig, described in the following section, will allow to identify stiffness and damping coefficients as a function of geometric parameters and operating conditions. Dynamic testing will excite the gas film at multiple frequencies while the static testing will include force and displacement measurements at 0 Hz.

Test Rig Description

The flat plate test rig for this experiment is shown below in Figure 2. The test rig consists of two parallel plates in very close proximity to one another. The top plate, houses the porous carbon thrust bearing and provides the means for pressurizing it. Once pressurized, a thin film of gas is created between the two plates. The bottom plate is flexibly mounted to the top plate via four turnbuckle assemblies and is connected to an electrohydraulic shaker capable of oscillating and modulating the gas film (i.e. induce relative motion between the two plates).

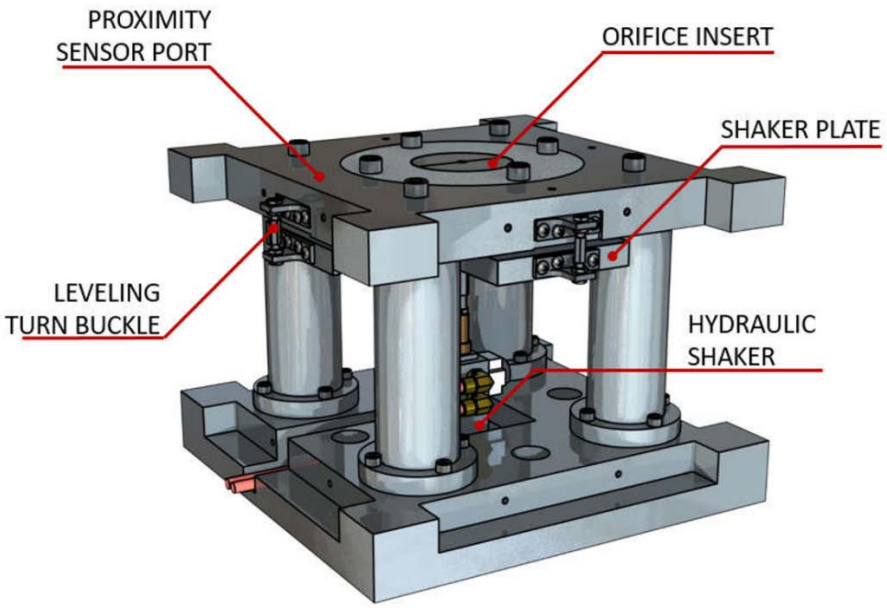

FIGURE 2: Flat Plate Test Rig

Test Rig Base

The test rig was mounted to a large base with t-slots using four sets of t-slot nuts and bolts. The base was then bolted down to an optic table to ensure that no outside vibrations or movements will impact the readings from the experiment. Fastening the base to the optical table presented a problem that had not been anticipated. Given that the test rig base weighs approximately four hundred and fifty pounds, a simple way to lift and carry the large base onto the optical table had not been considered when designing the test rig. In order to lift the base, a thick piece of steel with a thread through the middle was placed within the middle t-slot. An eye bolt with straps attached to a forklift was then threaded into the steel plate to lift the large base. A simple way to avoid this in the future is to design a couple of threaded holes directly into the top surface of the base. This design would be a much safer method of lifting the large base while also reducing the time and manpower required. Figure 3 shows a drawing of the base plate for the flat plate test rig.

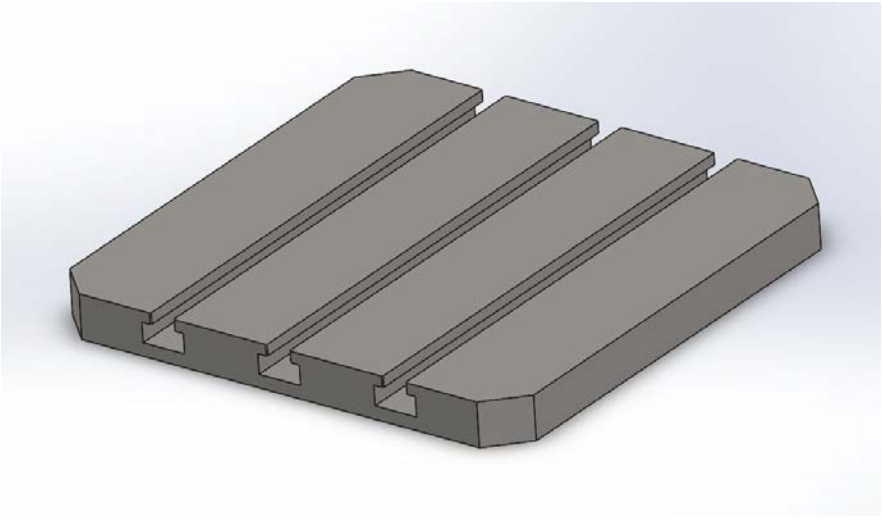

FIGURE 3: Test Rig Base Plate

Top Portion

The rig utilizes four columns to separate the top and bottom portions. The top portion houses the porous carbon gas delivery system and the static and dynamic plates. The dynamic plate is suspended from the upper portion of the test rig by four turnbuckle style rods and brackets. These rods are designed to level and maintain parallelism between the static and dynamic plates. Figure 4 shows the design of the turnbuckle assembly:

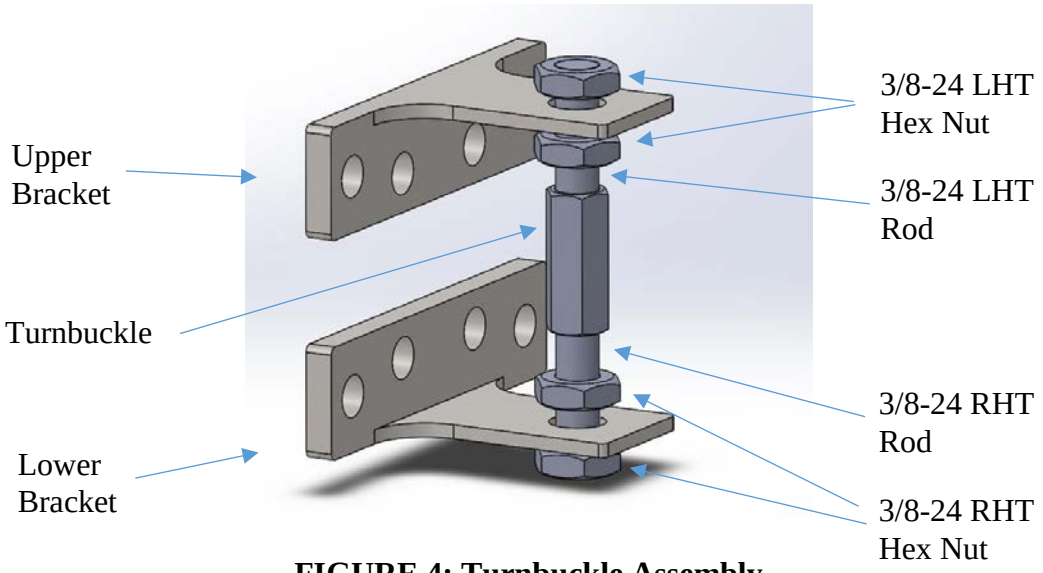

FIGURE 4: Turnbuckle Assembly

The upper bracket mounts to the top portion of the test rig while the bottom bracket mounts to the dynamic plate, acting as flexible cantilever beam elements. Since one rod in the turnbuckle is left-hand threaded while the other is right-hand threaded, turning the turnbuckle will cause the brackets to either move closer together or further apart. In this way, the turnbuckles can be used to manipulate the clearance between the two plates until the desired height is achieved.

The top portion of the test rig also contains the porous carbon thrust bearing. This bearing is circular and is positioned within the orifice insert shown in Figure 2. Figure 5 shows a detailed

description of the orifice insert. The insert consists of a top plate, a middle plate, and the air bearing. The middle plate contains a groove cut into the side to allow for plastic tubing to feed air to the bearing.

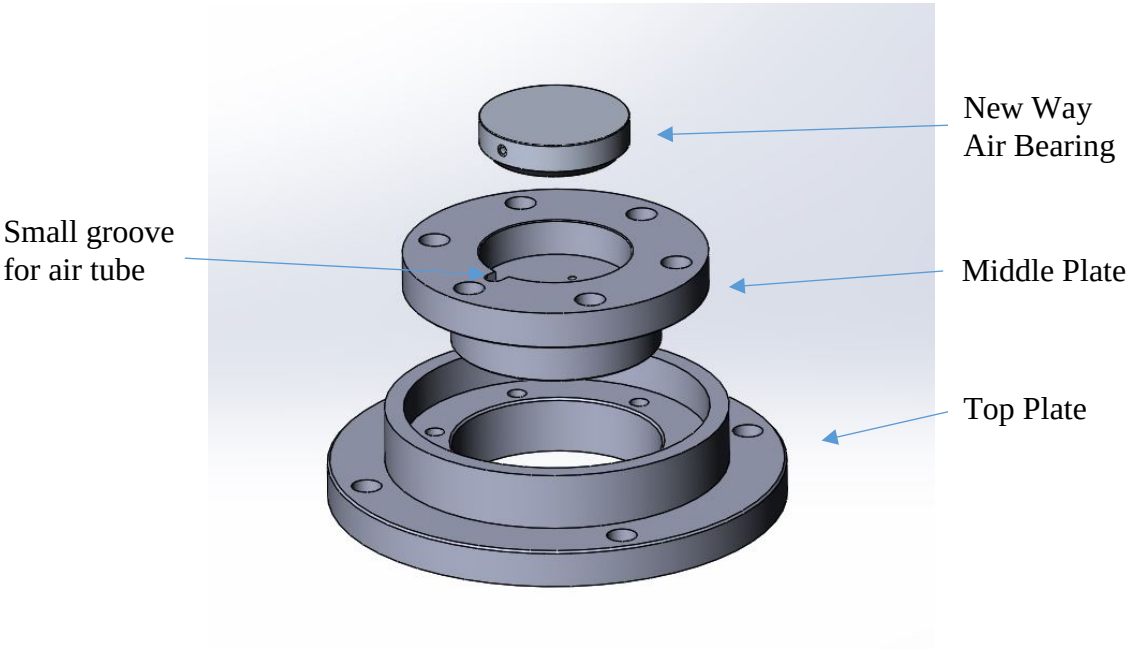

FIGURE 5: Orifice Insert

Bottom Portion

The bottom portion contains an electrohydraulic exciter head manufactured by XCITE Systems Corporation (P/N 1106-4-T/C) used to control the shaker plate. The purpose of the hydraulic exciter head is to create small oscillations in the shaker plate, exerting dynamic loads onto the thin gas film. The oscillations will only be implemented in the dynamic portion of the test and will be absent during the static testing.

While designing the bottom portion of the test rig, small grooves had to be put into place to allow for the hydraulic hoses feeding the hydraulic shaker to pass through. However, while assembling the rig, it was found that the groove was not shallow enough to allow for the hose to

clear the test rig base due to the height of the fittings on the exciter head. In order to overcome this, a thin aluminum spacer had to be machined to raise the exciter head just enough to clear the small groove.

Instrumentation

A flow meter placed between the air supply and the test rig measures the mass flow of air into the porous carbon pad. A load cell within the hydraulic shaker will be used during static testing to determine the constant force applied while a separate load cell will be used to more accurately measure the dynamic load during dynamic testing. Four proximity probes, shown in Figure 2, will be measuring the relative position and motion between the two plates, which will represent the thickness of the gas film. An accelerometer attached to the shaker plate will measure the acceleration of the motion of the shaker plate. This accelerometer is only operational during the dynamic testing portion. Lastly, a pressure sensor is utilized to measure the inlet pressure to the bearing and determine the ratio between the air supply feeding into the porous carbon pad and atmospheric pressure. This pressure sensor will be used in conjunction with a pressure regulator just upstream of the sensor that will enable the flow rate to be adjusted.

Test Preparation

In order to ensure the accuracy of collected data, all equipment used were calibrated prior to being assembled into the test rig. The most critical of these were the four proximity probes placed around the upper portion of the test rig. The proximity probes were calibrated by fixing each one at a set vertical distance from a stainless-steel plate. A -24V supply was provided to the probes and the vertical distance to the stainless-steel plate was varied 0.080”. The output voltage was measured using a voltmeter and data points were taken in increments of 0.001”. The sensitivities of the proximity probes were found to be between 268 and 272 mV/mil. These allow

to accurately measure the displacement of the shaker plate during the experiment. Figure 6 shows the calibration graphs for each of the probes.

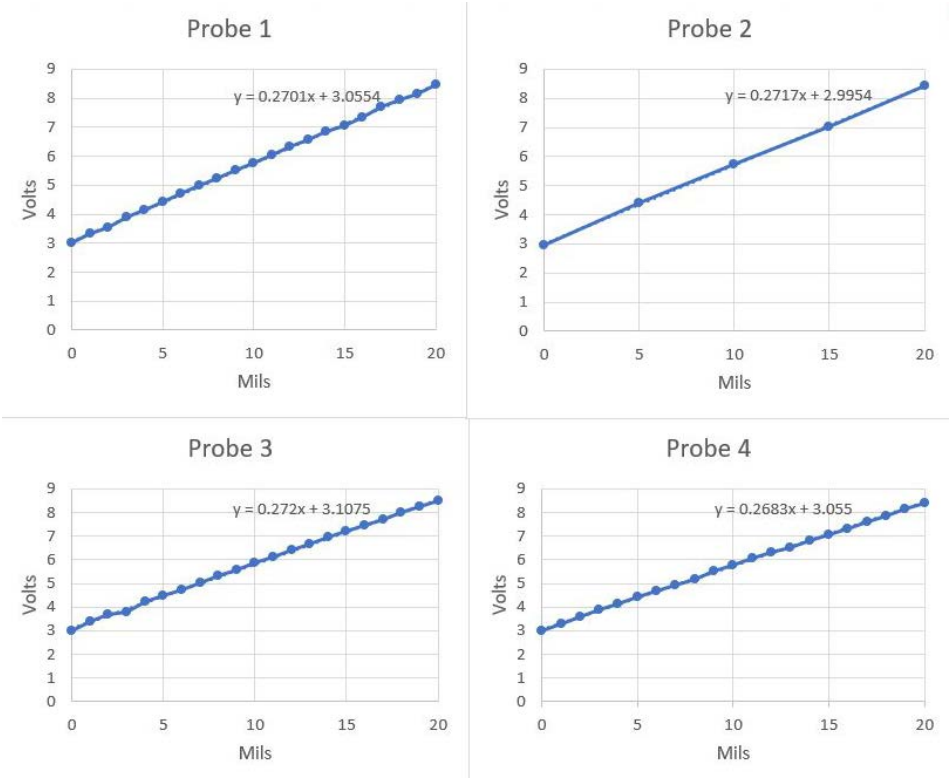

FIGURE 6: Proximity Probe Calibration Results

It is important to note that the sensitivity of about 270 mV/mil measured differed from the sensitivity of 200 mV/mil stated in the manual from the vendor for plain carbon steel. It shows that the probes will provide a different reading based on the material from which it is measuring distance. The uncalibrated sensitivity of 200 mV/mil will produce inaccurate results.

Subsequently, the shaker plate must be put in place (i.e. parallel faces) with the thrust bearing prior to testing. Once the proximity probes are calibrated and installed into the flat plate test rig, the shaker plate was installed and suspended from the turnbuckle assemblies. Each proximity probe measures vertical distance to the shaker plate. By analyzing the voltage signal of

each probe, it can be seen which side of the shaker plate is furthest from the carbon pad and which side is closest. Using the turnbuckles, the height of the shaker plate can be adjusted at four different locations.

CHAPTER III

SIMULATION RESULTS / FUTURE TESTING

Test Setup

Shop air is supplied to the test rig using standard shop air (max pressure of 120 psia) and air is supplied to the carbon pad using ¼-inch tubing and a series of valves. A standard ball valve is used to open and close the flow of air to the test rig while a pressure regulator is used to control the amount of air that can flow to the rig. Prior to passing through the pressure regulator, air passes through an air filter and a desiccant air dryer to clean and remove moisture from the air. Lastly, a flow meter is placed before the carbon pad to measure the mass flow of air entering the carbon pad.

Hydraulic fluid (Mobil DTE-24) is supplied to the exciter head using XCITE Systems Corporation's compatible Master Controller (P/N 1104-MOD4) and hydraulic pump (P/N 1201B-460-60). Hydraulic fluid is fed and returned between the hydraulic pump and the exciter head using 3/8-inch hoses. All operational commands for the pump are given by the master controller.

The majority of signals are sent and retrieved by National Instruments' NI PXIe-1082. The PXI receives signals from the proximity sensors, the accelerometer, the pressure sensor, and XCITE System's Master Controller in the form of voltages. The Master Controller sends the PXI signals on both the load cell reading and the excitation frequency. For static testing, it is assumed that enough time has passed such that the system is considered stable and all transients have died out. Therefore, the accelerometer and excitation frequency data are neglected. The PXI will also send signals to the pressure regulator to control the mass flow of air to the carbon pad. The

applied load and excitation frequency, although also read by the PXI, are controlled by knobs on the Master Controller. Both the Master Controller and the PXI are placed in a room adjacent to the test cell in which testing takes place, with a window positioned to observe the test rig. Figure 7 depicts a schematic of the test setup.

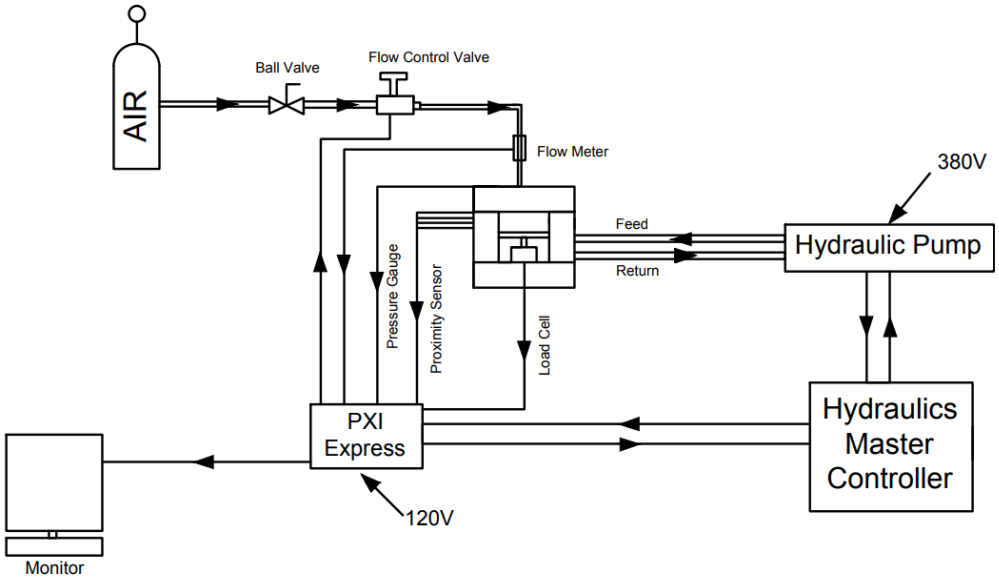

FIGURE 7: Test Schematic

Proposed Static Test Procedure

As mentioned in the *Methods* section, the stiffness coefficient will have contributions from both the gas films and the turnbuckle assemblies. In order to get an accurate characterization of the static performance of the gas film, the stiffness of the turnbuckles will first be determined. This is done by measuring the force on the load cell as the shaker plate is displaced upwards while no air is flowing through the bearing. The force will tend to linearly increase as the shaker plate approaches the bearing. The shaker plate will then be displaced all the way until it touches the bearing, and then backed off again. The measurements from the load cell and the proximity probes should result in a graph as shown in Figure 8:

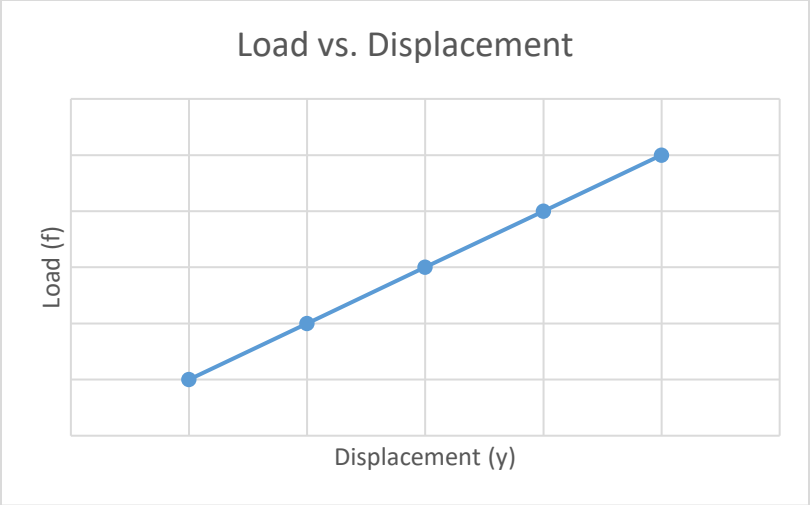

FIGURE 8: Sample Load Vs. Displacement Graph

The slope of the resulting graph represents the stiffness contribution of the turnbuckle, K_{tb}.

After the turnbuckle stiffness has been found, the gas film stiffness can then be calculated. This is done in a similar manner to calculating the turnbuckle stiffness, with the exception that air is now flowing through the gas bearing. The control valve is set to control the flow rate of air through the bearing while the gap between the shaker plate and the bearing shows no initial loading due to the flow rate. Next, the gap between the shaker plate and the bearing will decrease at linearly proportional increments. The operator should only notice the static forces from the turnbuckle acting on the plate while monitoring the initial load. At some gap between the bearing and the shaker plate, Y_1 the load cell will begin to measure resistance from the gas film. This can be seen graphically in Figure 9 when the force vs. displacement curve begins to deviate from the initial curve with no flow:

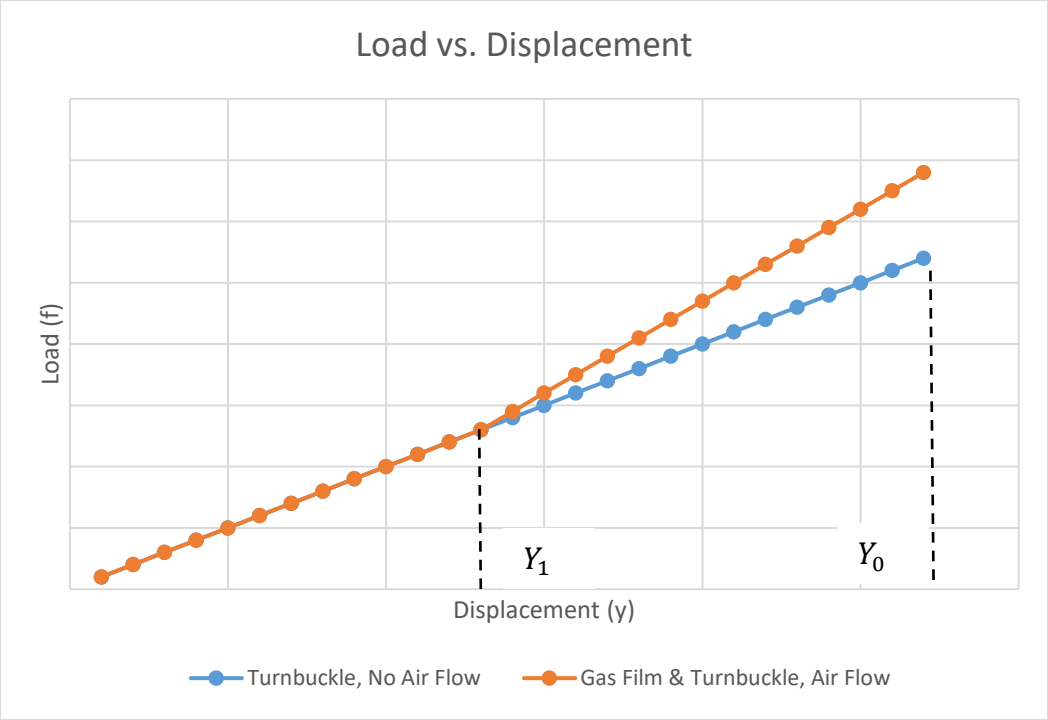

FIGURE 9: Theoretical Load Vs. Displacement Graph Illustrating Contributions of Gas Film and Turnbuckle

Data will be recorded until the shaker plate has touched the porous carbon bearing at Y_0. Taking the slope of the above Gas Film and Turnbuckle curve gives the stiffness coefficient of the gas film. Stiffness coefficients are found at a range of input pressures. For this project, the range of pressure used corresponds to the manufacturer's recommended range of operation for the porous carbon bearing. The specific range for the bearing used in this experiment is between 60 psi and 80 psi.

Static Test Simulation Results

Turnbuckle Assembly FEM Analysis

The turnbuckle assembly was modeled in SolidWorks and simulated in ANSYS to calculate a theoretical value for the turnbuckle stiffness coefficient K_{tb}. Figure 10 shows the mesh generated using ANSYS:

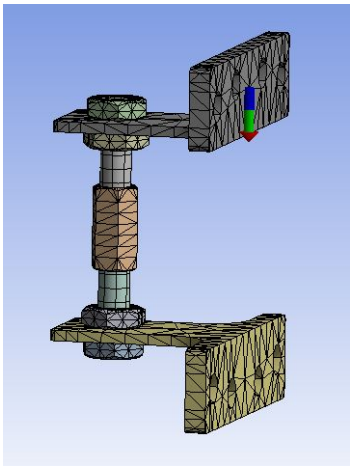

FIGURE 10: Turnbuckle Assembly Mesh (Undeformed State)

The upper bracket in Figure 10 was fixed while the lower bracket was displaced a total of 0.080 inches, the range of displacement that the proximity probes can measure. Using ANSYS, a reaction force is measured at the fixed end of the assembly. In order to get the total force applied to the turnbuckle assembly, the reaction force is multiplied by two to account for the reaction force of the lower bracket. Figure 11 shows the turnbuckle after deformation in the ANSYS simulations.

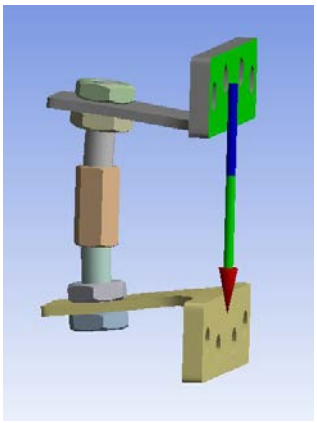

FIGURE 11: Turnbuckle Assembly (Deformed State)

Figure 12 shows the resulting data from simulating the turnbuckle assembly in ANSYS.

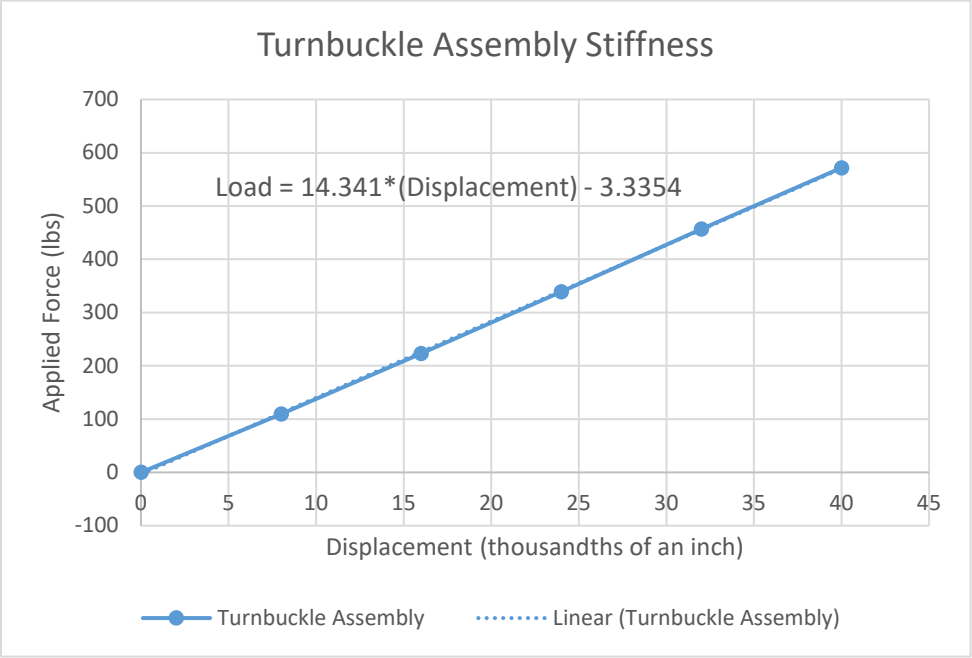

FIGURE 12: Turnbuckle Assembly Stiffness Calculation

Data after a displacement of 0.050 inches began to exhibit nonlinear behavior. This data was ignored due to the fact that the difference between Y_0 and Y_1 is likely much less than 0.050 inches. Data before reaching a displacement of 0.050 inches resulted in a linear plot. The stiffness

is then taken to be the slope of this linear plot, 14,341 lbf/in. It is important to note that this is the stiffness of one turnbuckle assembly while the actual experiment will contain four turnbuckles. Multiplying this value by four gives 57,364 lbf/in, an estimate for the turnbuckle contribution to the stiffness coefficient K_{tb}.

Performance data for the porous carbon air bearing can be found online on the manufacturers' website (New Way Bearings). The carbon air bearing begins to provide significant resistance when a guide surface is displaced up to within 0.001 inches of the face of the bearing. This means that during operation, the thickness of the gas film is likely about one fifth the thickness of a human hair. This analysis will therefore focus on a displacement range of 0.001 inches. Figure 13 shows the performance curve data taken from the manufacturer's website.

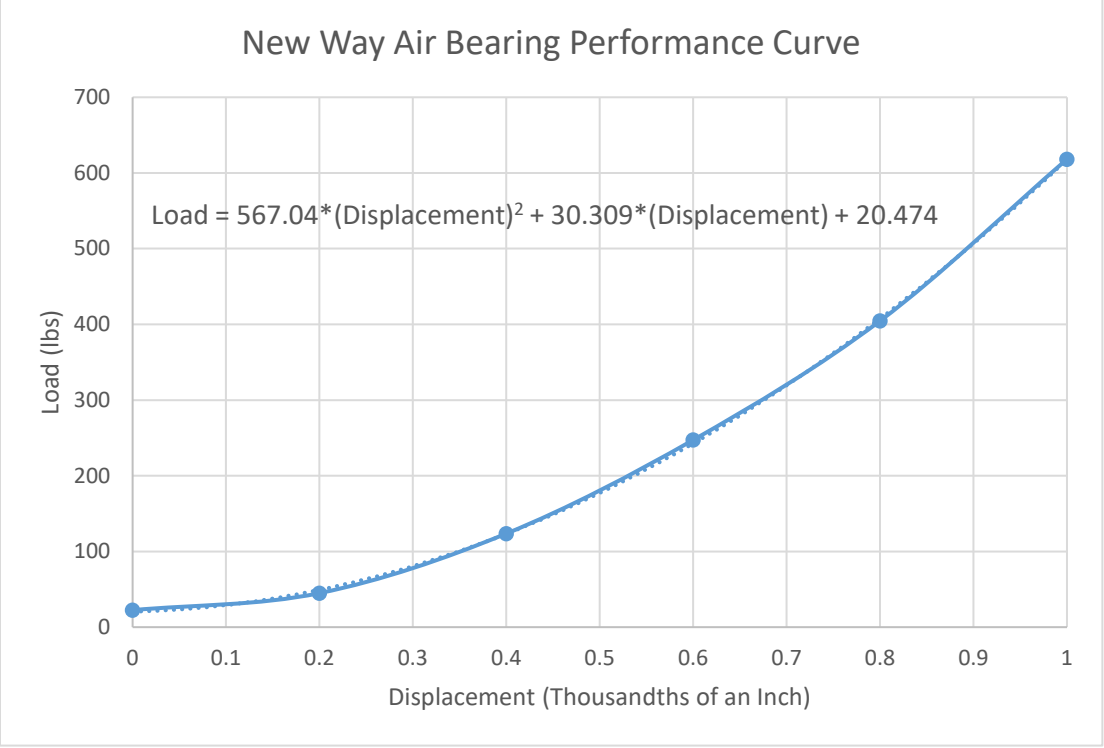

FIGURE 13: New Way Air Bearing Performance Curve [6]

The stiffness for the air bearing therefore differs from the stiffness of the turnbuckle by showing a nonlinear response to an applied load over a displacement of 0.001 inches. Figure 14 shows the stiffness of the gas film as a function of displacement calculated using the performance curve in Figure 13.

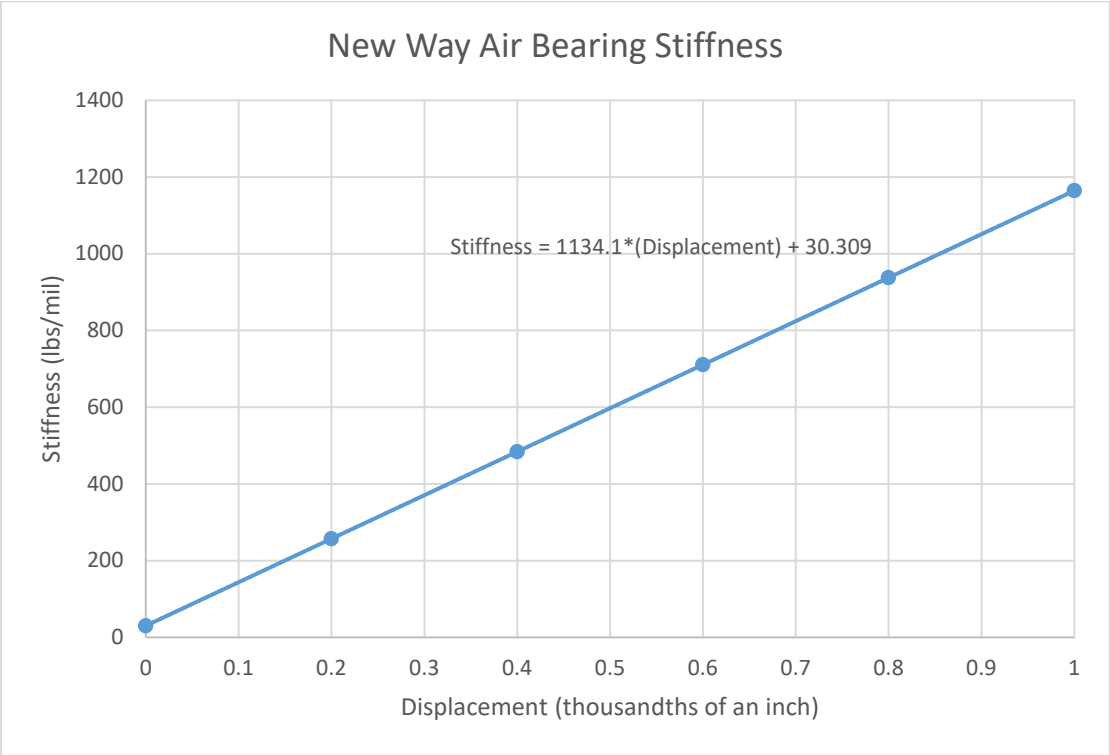

FIGURE 14: Stiffness of New Way Air Bearing [6]

The turnbuckle assembly can be adjusted so that the 0.001-inch displacement range during testing will fall within the linear portion of the performance curve. The stiffness contribution of 57,364 lbf/in will be verified experimentally and subtracted from the overall system stiffness to obtain the porous carbon gas film stiffness following Equation 2. By combining the stiffness vs, displacement curves of both the turnbuckle assemblies and the gas film, an estimate of overall stiffness readings is presented in Figure 15.

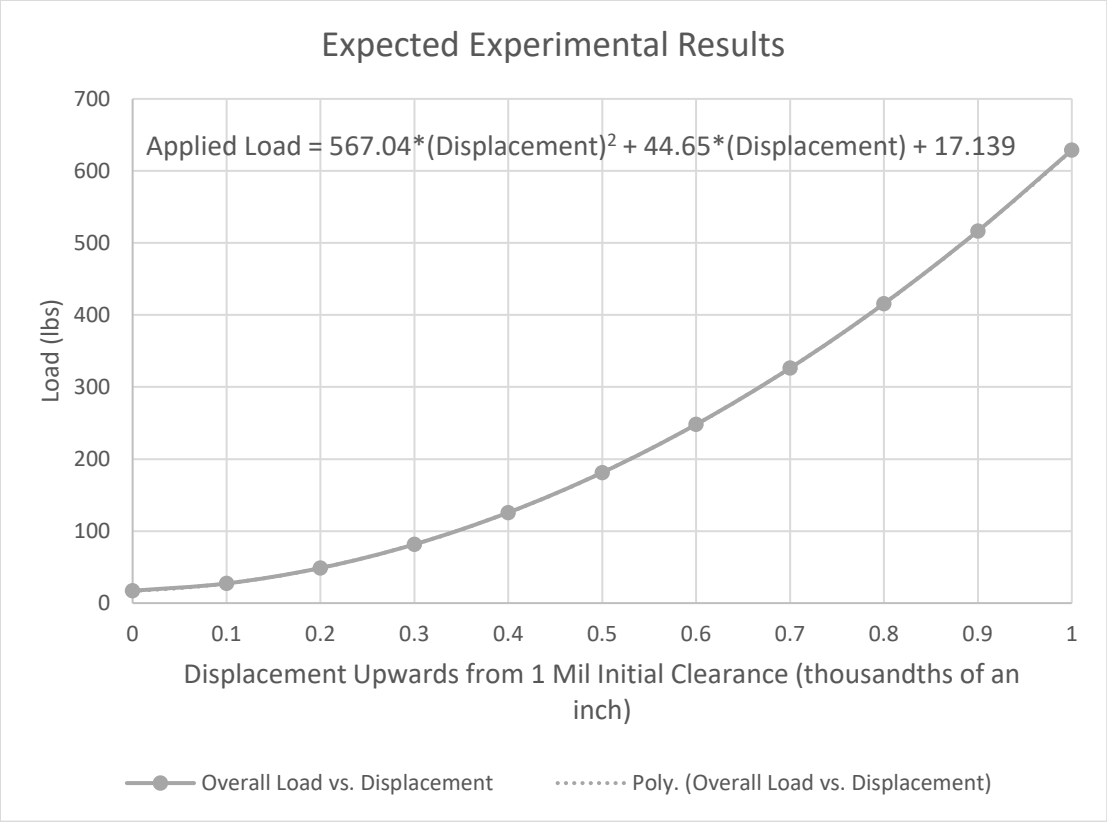

FIGURE 15: Estimate of Experimental Results

Proposed Dynamic Test Procedure

Characterizing the dynamic properties of the gas film will be accomplished in a similar fashion as the static testing, with some additional variables included. With the addition of an excitation frequency, damping is now present in the gas film. In order to extract stiffness and damping from the governing equation introduced in the *Methods* section, acceleration and velocity are required. This is measured using the accelerometer attached to the shaker plate. Testing results are also obtained for a range of excitation frequencies in addition to a range of inlet pressures as done in the static test procedure.

The testing procedure is executed in the same manner as the static testing procedure. The shaker plate is first set to a height of Y_1. The air is pressurized through the porous carbon bearing

and the exciter head begins to excite the shaker plate at a given frequency. The shaker plate is again displaced upwards until Y_0 is reached. Measurements of load, acceleration, and displacement, along with a numerical approximation for velocity, as a function of time will allow for stiffness and damping to be extracted.

CHAPTER IV

CONCLUSION

A test rig and an experimental methodology for characterizing the static and dynamic performance of aerostatic porous carbon bearings is presented. The aerostatic film is modeled as linear stiffness and damping coefficients considering small dynamic motions. The experimental methodology for identifying the static and dynamic coefficients is described along with numerical simulation of system static stiffness results.

The numerical results represent an estimate of the system static stiffness coefficients in lieu of actual experimental results. The turnbuckle stiffness is linear over the expected gas film range of motion, while the gas film exhibits a nonlinear stiffness coefficient. Nonetheless, the dynamic stiffness coefficient and damping for small dynamic perturbation is expected to be a linear coefficient. The turnbuckle stiffness coefficient will be measured experimentally and subtracted from both the static and dynamic system force coefficients to obtain the actual gas film stiffness and damping coefficients.

The proposed testing procedures discussed in the previous section will begin to take place during the week of April 16th, 2018. The research team expects to take about a month finalizing the results of the experiment.

Recommendations

The timeline of this project turned out much different than originally planned. Many unanticipated obstacles kept the research team from obtaining experimental data. Students undergoing similar research project should be made aware of these problems. The largest time delays for this project came because of waiting on outside vendors to supply the parts needed to

assemble the test rig. It is inevitable that there will be complications when dealing with many different vendors. For this project, the wrong pressure sensor was delivered and the grinder needed to add a good surface finish to the shaker plate was delayed significantly, to name a few problems. Students should allot additional time to the project for unanticipated problems such as these and plan ahead with other tasks that can be completed in the meantime. This will help ensure that the research project progresses along quicker.

REFERENCES

[1] Dellacorte, C., Valco, M. J., 2000, “Load Capacity Estimation of Foil Air Journal Bearings for Oil-Free Turbomachinery Applications,” Society of Tribologists and Lubrication Engineers, 43(4), pp. 795-801.

[2] Delgado, A., 2015, “Experimental Identification of Dynamic Force Coefficients for a 110 MM Compliantly Damped Gas Bearing,” Journal of Engineering for Gas Turbines and Power, 137(7), pp. 072502.

[3] Jacob, J.S., Yu, J.J., Bently, D.E., Goldman, P., “Air-Hammer Instability of Externally Pressurized Compressible-Fluid Bearings,” International Symposium of Stability Control of Rotating Machinery.

[4] Harnoy, A., 2003, Bearing Design in Machinery, Engineering Tribology and Lubrication, Marcel Dekker, Inc., New York, NY.

[5] Rowe, W.B., 2012, Hydrostatic, Aerostatic, and Hybrid Bearing Design, Elsevier Inc., Waltham, MA.

[6] “100mm Flat Round Air Bearing”, [Online]. Available: https://www.newwayairbearings.com/catalog/product/100mm-flat-round-air-bearings/. [Accessed: 8-Apr-2018].